ADVANCED FUNCTIONAL MATERIALS
www.afm-journal.de

White Organic Light-Emitting Diodes with Evenly Separated Red, Green, and Blue Colors for Efficiency/Color-Rendition Trade-Off Optimization

Shuming Chen, Guiping Tan, Wai-Yeung Wong, and Hoi-Sing Kwok**

A novel yellowish-green triplet emitter, bis(5-(trifluoromethyl)-2-*p*-tolylpyridine)(acetylacetonate)iridium(III) (1), was conveniently synthesized and used in the fabrication of both monochromatic and white organic light-emitting diodes (WOLEDs). At the optimal doping concentration, monochromatic devices based on 1 exhibit a high efficiency of 63 cd A^{-1} (16.3% and 36.6 lm W^{-1}) at a luminance of 100 cd m^{-2}. By combining 1 with a phosphorescent sky-blue emitter, bis(3,5-difluoro-2-(2-pyridyl)phenyl)-(2-carboxypyridyl)iridium(III) (FIrPic), and a red emitter, bis(2-benzo[*b*]thiophen-2-yl-pyridine)(acetylacetonate)iridium(III) ($Ir(btp)_2(acac)$), the resulting electrophosphorescent WOLEDs show three evenly separated main peaks and give a high efficiency of 34.2 cd A^{-1} (13.2% and 18.5 lm W^{-1}) at a luminance of 100 cd m^{-2}. When 1 is mixed with a deep-blue fluorescent emitter, 4,4′-bis(9-ethyl-3-carbazovinylene)-1,1′-biphenyl (BCzVBi), and $Ir(btp)_2(acac)$, the resulting hybrid WOLEDs demonstrate a high color-rendering index of 91.2 and CIE coordinates of (0.32, 0.34). The efficient and highly color-pure WOLEDs based on 1 with evenly separated red, green, blue peaks and a high color-rendering index outperform those of the state-of-the-art emitter, *fac*-tris(2-phenylpyridine)iridium(III) ($Ir(ppy)_3$), and are ideal candidates for display and lighting applications.

1. Introduction

White organic light-emitting diodes (WOLEDs) have been of considerable interest in recent years due to their potential applications in high-resolution, full-color displays and solid-state lighting.[1–15] Generally, to construct WOLEDs, two or three emitters that emit two complementally colors[1–4] or three primary colors[5–10] should be employed. For display applications, it is important that the generated white light can be separated into three primary colors with equal emission intensity after passing through the color filters.[11,12] To this end, the spectra of the WOLEDs should normally possess three evenly separated red (R), green (G) and blue (B) peaks that correspond to the transmission peaks of the R, G and B color filters. For lighting applications, the 1931 Commission International de L'Eclairage (CIE) coordinates of the white spectrum should be close to the equal-energy-white-point (i.e., (0.33, 0.33)) and the spectrum should cover the whole visible region in order to provide a high color-rendering capability for objects viewed under such white light. Thus, it is preferable to adopt a three-emitter system so that the resulting white spectrum can possess R, G and B components and a high color-rendering index (CRI).[5–10]

For a three-emitter system, the emitters must be carefully chosen. The emission spectra of the emitters should compensate each other so that the white spectrum generated can cover the whole visible region with a uniform emission intensity. For blue phosphorescent emitters, there are not many choices but to employ bis(3,5-difluoro-2-(2-pyridyl)phenyl)-(2-carboxypyridyl)iridium(III) (FIrPic), a sky-blue emitter with a central emission wavelength of 475 nm, due to the scarcity of deep-blue-phosphorescent emitters in the literature. It is common to adopt bis(2-benzo[*b*]thiophen-2-yl-pyridine)(acetylacetonate) iridium(III) ($Ir(btp)_2(acac)$), with a central emission wavelength of 616 nm, as a saturated red emitter. In order to generate the white spectrum with three evenly separated R, G and B peaks, the central emission wavelength of the green emitter should thus be located at (616 + 475)/2 = 545 nm. Commercially available green emitters such as *fac*-tris(2-phenylpyridine) iridium(III) ($Ir(ppy)_3$) or bis(2-phenylpyridine)(acetylacetonate) iridium(III) ($Ir(ppy)_2(acac)$), with a central emission wavelength of ≈512 nm, cannot meet this spectral requirement. WOLEDs employing the above-mentioned benchmark green emitters exhibit a low color-rendering capability due to the undesirable

S. Chen, Prof. H.-S. Kwok
Centre for Display Research and Department of Electronic and Computer Engineering
The Hong Kong University of Science & Technology
Clear Water Bay, Kowloon
Hong Kong, P. R. China
E-mail: eekwok@ust.hk
G. Tan, Prof. W.-Y. Wong
Department of Chemistry and Centre for Advanced Luminescence Materials
Hong Kong Baptist University
Waterloo Road, Kowloon Tong
Hong Kong, P. R. China
E-mail: rwywong@hkbu.edu.hk
S. Chen, G. Tan, Prof. W.-Y. Wong, Prof. H.-S. Kwok
Institute of Molecular Functional Materials
Areas of Excellence Scheme
University Grants Committee of HKSAR, P. R. China

DOI: 10.1002/adfm.201100895

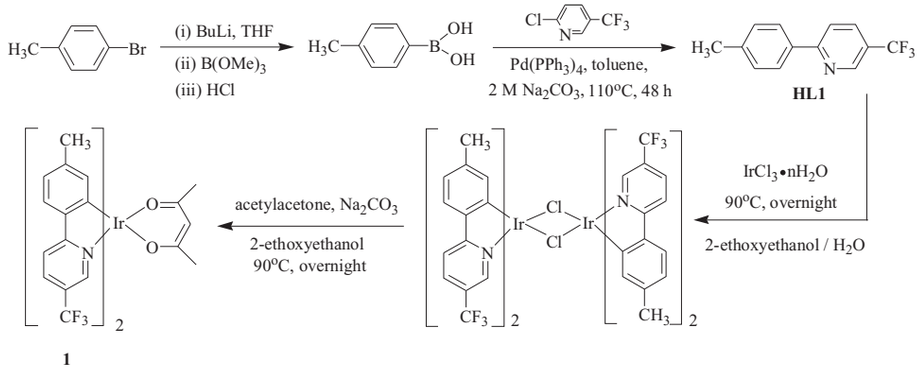

Scheme 1. Synthetic sketch leading to the iridium(III) heteroleptic complex **1**.

deep valley present between the R and G peaks.[5–10] To address this problem, one more yellow emitter[13] or even two more emitters[14] have been employed to achieve a good white-light spectrum, which inevitably increases the complexity of the system. It is thus necessary to develop new, efficient, phosphorescent, yellowish-green emitters with a central emission wavelength close to 545 nm, so that a broadband white spectrum with a uniform emission intensity covering the whole visible spectrum can be realized in a relatively simple three-emitter system. Previously, Park et al.[15] synthesized a high-energy-level yellowish-green phosphor for constructing WOLEDs in such a three-color stratagem. The resulting WOLEDs exhibited a moderate peak efficiency of 11.7%, 23.4 cd A^{-1} and 13.2 lm W^{-1} and showed a high CRI of 87, mainly due to the evenly separated R, G and B peaks, by adopting the yellowish-green dopant.

In this contribution, we easily synthesized a new yellowish-green emitter, **1**, with a central electroluminescence (EL) wavelength of 544 nm, for application in WOLEDs. Complex **1** possesses a high EL efficiency; for example, at an optimal doping concentration, monochromatic devices based on **1** exhibited a high luminance efficiency (LE) of 63 cd A^{-1} at a luminance of 100 cd m^{-2}, corresponding to an external quantum efficiency (EQE) of 16.3% and a power efficiency (PE) of 36.6 lm W^{-1}. Upon combination of **1** with FIrPic and $Ir(btp)_2(acac)$ in the active layer, the resulting electrophosphorescent WOLEDs showed three evenly separated peaks and gave a high efficiency of 34.2 cd A^{-1} (13.2% and 18.5 lm W^{-1}) at the relevant brightness level of 100 cd m^{-2}. By combining **1** with the deep-blue fluorescent emitter 4,4′-bis(9-ethyl-3-carbazovinylene)-1,1′-biphenyl (BCzVBi) and $Ir(btp)_2(acac)$, the resulting hybrid WOLEDs demonstrated a very-high CRI of 91.2 and CIE coordinates of (0.32, 0.34). The efficient WOLEDs demonstrated here, with separated R, G, and B peaks and high CRI, are ideal candidates for display and lighting applications.

2. Results and Discussion

2.1. Synthetic Strategies, Chemical Characterization and Thermal, Photophysical and Electrochemical Properties

Although heteroleptic iridium(III) complexes $Ir(C^N)_2(acac)$, with C^N = 5-trifluoromethyl-2-phenylpyridine ($Ir(CF_3\text{-}ppy)_2(acac)$), and 2′-*p*-tolylpyridine ($Ir(tpy)_2(acac)$) are known in the literature,[16] there have been no reports to date of the iridium(III) derivative with both CF_3 and CH_3 groups attached to the ppy ligand. The synthesis of **1** is shown in **Scheme 1**. The key ligand precursor is the 4-methylphenylboronic acid, synthesized from 4-bromotoluene, *n*-butyl lithium and trimethyl borate in a dry ice–acetone bath. **HL1** was conveniently synthesized from the palladium-catalyzed Suzuki cross-coupling of 2-chloro-5-trifluoromethylpyridine with the boronic acid derivative.[17] Then, $IrCl_3 \cdot nH_2O$ reacted with an excess of the **HL1** to give a chloride-bridged iridium(III) dimer. The dimer could be readily cleaved to the monomeric complex by replacing the bridging chlorides with acetylacetonate anion (acac) derived from the deprotonation of acetylacetone (Hacac) by sodium carbonate.[18] Purification of the mixture by preparative thin-layer-chromatography (TLC) plates furnished **1** as an air-stable orange powder in a high purity. All of the compounds were thoroughly characterized by NMR spectroscopy and fast-atom-bombardment mass spectrometry (FAB-MS). ^{1}H-NMR-spectroscopy data suggested that complex **1** was always in its pure stereoisomeric form, with one set of proton signals.

The thermal stability of **1** was evaluated using thermogravimetric analysis (TGA) measured under a nitrogen stream (**Table 1**). Complex **1** was thermally stable up to 327 °C, suggesting that it could be vacuum-evaporated to form a good-quality thin film.

The UV–vis and photoluminescence (PL) spectra of **1** were measured in CH_2Cl_2 solution (Table 1, **Figure 1**). The higher-energy absorption peaks below 350 nm were assigned to ligand-based spin-allowed $^1\pi$–π^* transitions. The weaker absorption peaks above 350 nm with lower extinction coefficients possessed substantial mixing of ligand-based $^3\pi$–π^* states, spin-allowed singlet metal-to-ligand charge-transfer (^{1}MLCT) and spin-forbidden triplet metal-to-ligand charge-transfer (^{3}MLCT) states. The spin-orbit coupling was enhanced by the presence of closely spaced π–π^* and MLCT states and the presence of the heavy-atom effect of the iridium(III) center.[19] Complex **1** emitted a strong phosphoresecence at 547 nm at 293 K (543 nm at 77 K). The slight blue shift was caused by solvent recorganization from a fluid solution to a rigid matrix when the temperature changed from 293 K to 77 K. The change of the solution phase impeded the stabilization of charge-transfer states before emission occurred; therefore, phosphorescence predominantly

Table 1. Photophysical, electrochemical and thermal data for complex 1.

Absorption[a]	Emission (CH_2Cl_2)		E_{ox} [V][d]	HOMO [eV][e]	LUMO [eV][f]	E_g [eV][g]	ΔT_{dec} [°C][h]
λ_{abs} [nm]	λ_{em} at 293 K/77 K [nm][b]	τ_P [μs][c]					
277 (3.74), 313 (2.30), 361 (0.46), 379 (0.30), 473 (0.09)	547/543 (0.47)	0.92	0.52	–5.32	–2.84	2.48	327

[a]In degassed CH_2Cl_2 at 293 K; molar extinction coefficient ε values ($\times 10^4$ M^{-1} cm^{-1}) are shown in parentheses; [b]The phosphorescence quantum yield, Φ_P, at 293 K is shown in parentheses against Ir(ppy)$_3$ (Φ_P = 0.40), λ_{ex} = 400 nm; [c]Triplet lifetime at 293 K; [d]0.1 M [Bu_4N]PF_6 in tetrahydrofuran (THF), versus Fc/Fc$^+$ couple; [e]HOMO = $-(E_{ox} + 4.8)$; [f]LUMO = HOMO + E_g; [g]Estimated from the onset wavelength of the optical absorption; [h]At a heating rate of 5 °C min^{-1} under N_2.

of the ^{3}MLCT nature took place at higher energy.[20] The PL emission maximum of **1** was between that for (Ir(CF$_3$-ppy)$_2$(acac)) (554 nm) and (Ir(tpy)$_2$(acac)) (512 nm). Compared with the emission spectrum at room temperature, the PL spectrum at 77 K showed an apparent vibrational fine structure (with a shoulder peak at about 572 nm), and this structured emission revealed that the mixing between the ^{3}MLCT and $^3\pi$–π^* levels was so effective that an almost ligand-centred emission was observed upon freezing the matrix.[21] The phosphorescence quantum yield (Φ_P) of **1** in CH_2Cl_2 solution excited at 400 nm was 0.47, which is comparable to the Ir(ppy)$_3$ standard (Φ_P = 0.40). The short phosphorescence lifetime, τ_P, of 0.92 μs indicates a weaker triplet-triplet annihilation, which reduces the chance of a decay in the efficiency of the devices.[22]

The electrochemical behavior of **1** was investigated by cyclic voltammetry using ferrocene as the internal standard and the results are listed in Table 1. A reversible wave was found in the anodic scan ($E_{1/2,ox}$ = 0.52 V), which can be assigned to the Ir^{IV}/Ir^{III} oxidation.[23] The highest-occupied-molecular-orbital (HOMO) energy level was estimated from the oxidation couple to be –5.32 eV, with respect to the energy level of the ferrocene reference (4.8 eV below the vacuum level).[24]

2.2. Characterization and Optimization of 1-Doped Monochromatic OLEDs

To optimize the device performance, two kinds of device with the following structures were fabricated and compared: a) type 1: ITO/NPB (60 nm)/2–7% **1**:CDBP (20 nm)/TAZ (40 nm)/LiF (1 nm)/Al (100 nm); and b) type 2: ITO/NPB (60 nm)/4% **1**:CBP (20 nm)/TPBi (40 nm)/LiF (1 nm)/Al (100 nm) (where ITO = indium tin oxide; NPB = *N*,*N*′-bis(naphthalen-1-yl)-*N*,*N*′-bis(phenyl)-benzidine; CDBP = 4,4′-bis(carbazol-9-yl)-2,2′-dimethylbiphenyl; TAZ = 3-(4-biphenyl)-4-phenyl-5-*tert*-butylphenyl-1,2,4-triazole; CBP = 4,4′-bis(carbazol-9-yl)biphenyl; and TPBi = 2,2′,2″-(1,3,5-benzinetriyl)-tris(1-phenyl-1-*H*-benzimidazole)). In the type-1 devices, the CDBP host material and the TAZ exciton-blocking material were chosen to effectively confine the excitons within **1**. For comparison, CBP as host material and TPBi as exciton-blocking material were chosen in the type-2 device. To find out the best doping level, the doping concentration of **1** was varied from 2 wt% to 7 wt%. Meanwhile, green OLEDs based on the commercial green emitter Ir(ppy)$_3$ with a type-3 structure: ITO/NPB (60 nm)/7% Ir(ppy)$_3$:CDBP (20 nm)/TAZ (40 nm)/LiF (1 nm)/Al (100 nm) were also fabricated and compared. **Figure 2**a displays the typical current-density–voltage–luminance (*J*–*V*–*L*) curves for the devices. All of the devices with CDBP as the host and TAZ as the exciton-blocking layer exhibited similar *J*–*V*–*L* characteristics. At higher doping concentrations, the current density decreased slightly, indicating that more excitons were trapped by the phosphor, **1**, at higher doping levels. The devices with CBP as the host and TPBi as the exciton-blocking layer exhibited a substantially larger current density at a certain voltage, mainly due to the lower triplet energy level of the CBP and TPBi compared with that of CDBP and TAZ, resulting in a lower carrier-injection barrier and hence a larger current density.[25] Figure 2b shows the current-efficiency–luminance characteristics of the devices. It is clear that the efficiency of the devices with CDBP as the host and TAZ as the exciton-blocking layer increased with increasing doping concentration up to a certain level and then decreased when the doping level was increased. For example, at a luminance of 1000 cd m^{-2}, the LE increased from 54 cd A^{-1} for a doping concentration of 2 wt% to 61.6 cd A^{-1} for a doping concentration of 4 wt% and then decreased to 51.8 cd A^{-1} for a doping concentration of 7 wt%. Thus, the optimal doping concentration was around 4 wt%. At lower doping concentrations, the energy transfer from the host to **1** may not be complete, while at higher doping concentrations, triplet-triplet annihilation may reduce the efficiency. At the optimal doping concentration of 4 wt%, devices with CDBP as the host and TAZ as the exciton-blocking layer exhibited a substantially higher LE of 61.6 cd A^{-1} at 1000 cd m^{-2}, compared with 40 cd A^{-1} at 1000 cd m^{-2} for the devices with CBP as the host and TPBi as the exciton blocking layer, which is likely to be due to the higher triplet energy levels of CDBP (3.0 eV) and TAZ (2.7 eV),

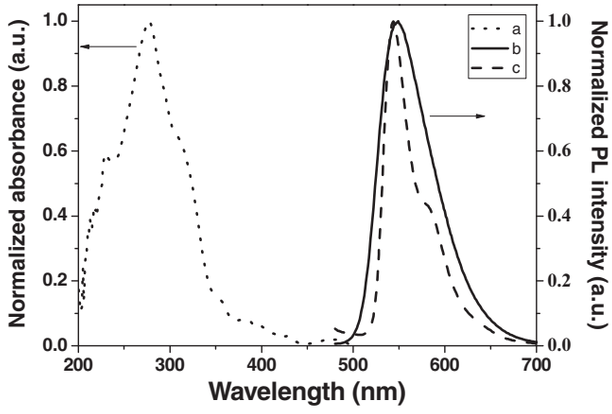

Figure 1. Optical absorption and photoluminescence spectrum of **1** in CH_2Cl_2 (a: UV spectrum at 293 K; b: PL spectrum at 293 K; c: PL spectrum at 77 K).

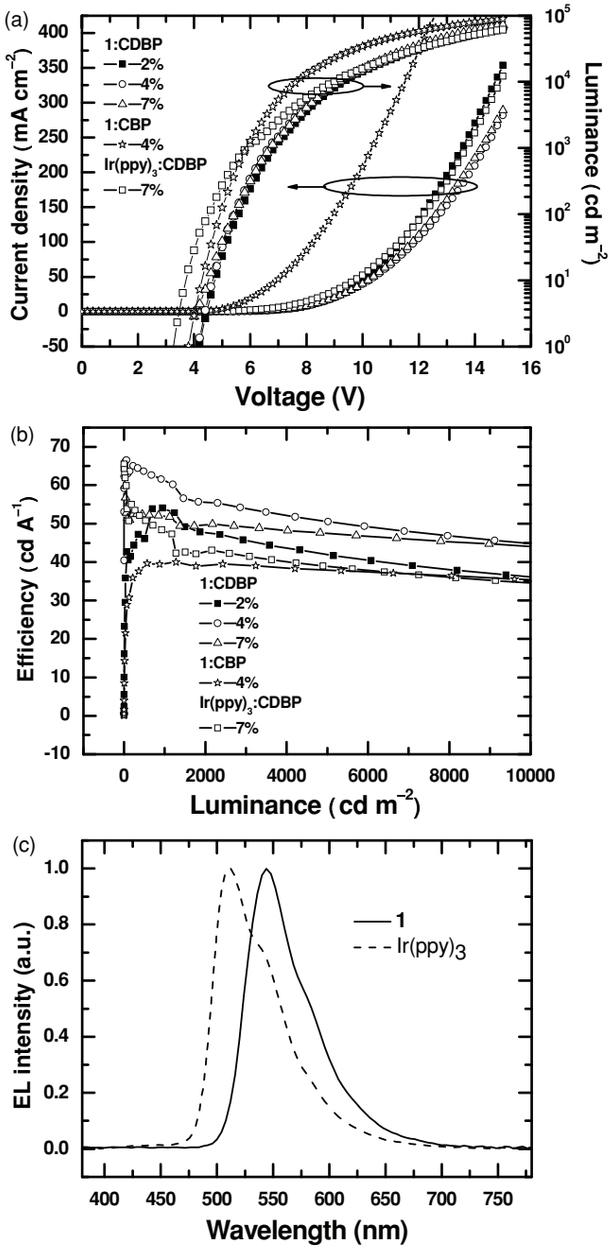

Figure 2. a) Current-density–voltage–luminance characteristics of the devices based on **1** and $Ir(ppy)_3$. b) Efficiency–luminance characteristics of the devices based on **1** and $Ir(ppy)_3$. c) EL spectra of the devices based on **1** and $Ir(ppy)_3$.

compared with those of CBP (2.6 eV) and TPBi (2.67 eV), respectively, resulting in better triplet exciton confinement and hence higher efficiency.[25] The performance of the devices with the commercial green emitter $Ir(ppy)_3$ is also included for comparison. It was noted that the efficiency of the devices with **1** was significantly higher than that of the devices with $Ir(ppy)_3$. Most likely, the improved device efficiency of **1** can be traced to the steric hindrance of both CF_3 and methyl groups.[26] For example, at a luminance of 1000 cd m^{-2}, the LE of the devices with 4 wt% **1** reached 61.6 cd A^{-1}, which is 1.27 times higher than the 48.4 cd A^{-1} for the devices with $Ir(ppy)_3$. The key characteristics of the devices are summarized in **Table 2**. Figure 2c shows the EL spectra of the devices with **1** and $Ir(ppy)_3$. Complex **1** emitted a yellowish-green color with a central emission wavelength of 544 nm, which was red shifted by 32 nm compared with that for $Ir(ppy)_3$ at 512 nm. The yellowish-green emission color and excellent performance of **1** suggest the good potential of employing **1** as the emitter for the construction of efficient WOLEDs showing evenly separated R, G and B colors.

2.3. Fabrication and Characterization of Efficient WOLEDs with Evenly Separated Red, Green and Blue Peaks

The excellent performance of **1** prompted us to explore its application in WOLEDs. A series of phosphorescent WOLEDs were fabricated with the structure: ITO/NPB (40 nm)/6% $Ir(btp)_2(acac)$:CDBP (10 nm)/4% **1**:CDBP (0–4 nm)/12% FIrPic:CDBP (5 nm)/TAZ (40 nm)/LiF (1 nm)/Al (100 nm), where 10 nm-thick CDBP doped with 6 wt% $Ir(btp)_2(acac)$ served as the red-emitting layer and 5 nm-thick CDBP doped with 12 wt% FIrPic worked as the sky-blue-emitting layer. The thickness of the yellowish-green-emission layer, **1**:CDBP, was varied from 0 to 4 nm in order to tune the purity of the white spectrum as well as the device efficiency. **Figure 3**a shows the spectra of the devices with a 0 nm thickness of the **1**:CDBP layer. The resulting white spectra exhibited two main peaks centered at 475 nm and 616 nm, which arose from the emission of the FIrPic and the $Ir(btp)_2(acac)$, respectively. Though the CIE coordinates of (0.35, 0.38) are very close to the equal-energy-white-point, such white spectra may not find application in display or lighting, mainly due to the lack of a green component. For display applications, the green color is mainly resolved from the tail of the sky-blue emission after such white light passes through the color filter, which would result in a weak green-light intensity as well as poor color saturation. For lighting applications, the lack of green peaks in the spectrum leads to a poor color-rendering capability (i.e., green and

Table 2. Key performance characteristics of devices based on **1** and $Ir(ppy)_3$.

Structure	Phosphor dopant	V_{on} [V]	L_{max} @ 15 V [cd m^{-2}]	η_{ext} [%]	η_L [cd A^{-1}]	η_P [lm W^{-1}]	λ_{max} [nm]
1:CDBP/TAZ	2%	4.2	62921	10.5[a], 14.0[b]	40.5, 54.0	22.7, 24.9	544
	4%	4.2	63059	16.3[a], 15.9[b]	63.0, 61.6	36.6, 29.3	544
	7%	4.2	71685	13.3[a], 13.4[b]	51.4, 51.8	39.9, 23.9	544
1:CBP/TPBi	4%	3.8	89339	8.2[a], 10.6[b]	30.8, 40.0	19.3, 20.9	544
$Ir(ppy)_3$:CDBP/TAZ	7%	3.4	61214	14.5[a], 13.9[b]	50.7, 48.4	34.6, 26.2	512

[a]Values collected at 100 cd m^{-2}; [b]Values collected at 1000 cd m^{-2}.

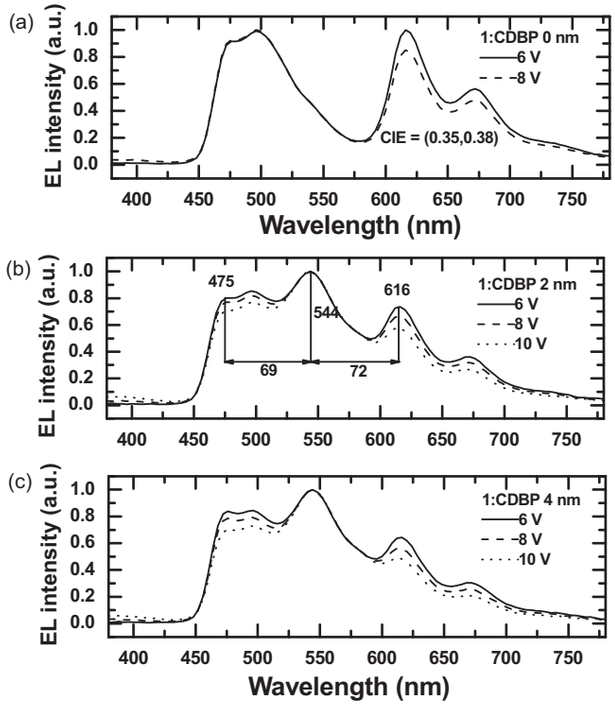

Figure 3. a–c) EL spectra of WOLEDs with **1**:CDBP yellowish-green-emission layers with thicknesses of 0 nm (a), 2 nm (b) and 4 nm (c).

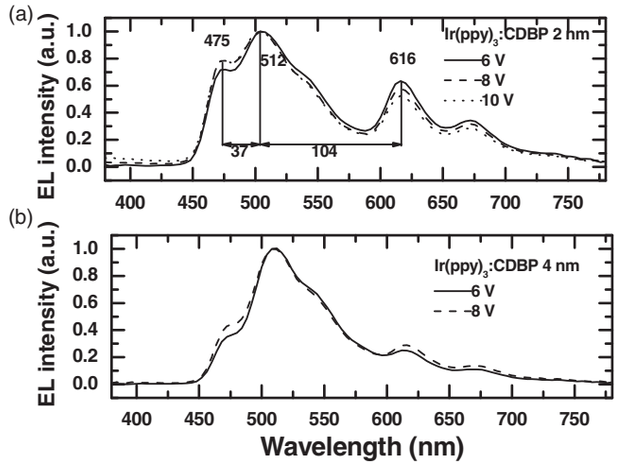

Figure 4. a,b) EL spectra of WOLEDs with $Ir(ppy)_3$:CDBP green-emission layers with thicknesses of 2 nm (a) and 4 nm (b).

yellow objects cannot be correctly rendered under the illumination of such white light). Thus, it is necessary to remedy this deficiency in such white spectra with a yellowish-green color element. By employing a 2 nm thickness of **1**:CDBP as the yellowish-green emission layer, a new peak, centered at 544 nm, originating from **1** was clearly observed. With the compensation of the yellowish-green emission, the resulting white spectra exhibited three evenly separated peaks, as shown in Figure 3b. The spectra also demonstrated moderate color stability. With the increase of the driving voltage, the blue and red peaks decreased slightly in intensity with the CIE coordinates changing from (0.35, 0.46) at 6 V to (0.34, 0.46) at 8 V, which signifies that more excitons recombined in the yellowish-green region with an increased driving voltage. It was also noted that the red emission intensity decreased slightly when the thickness of the yellowish-green emission layer was increased, as depicted in Figure 3c, resulting in the CIE coordinates changing from (0.35, 0.46) at 6 V for the devices with a 2 nm thickness of **1**:CDBP to (0.34, 0.46) at 6 V for the devices with a 4 nm thickness of **1**:CDBP. However, the EL efficiency was enhanced significantly on increasing the thickness of the yellowish-green emission layer (vide infra).

For comparison, WOLEDs using the commercial benchmark green-emitter $Ir(ppy)_3$ were also fabricated with the device structure: ITO/NPB (40 nm)/6% $Ir(btp)_2(acac)$:CDBP (10 nm)/7% $Ir(ppy)_3$:CDBP (2–4 nm)/12% FIrPic:CDBP (5 nm)/TAZ (40 nm)/LiF (1 nm)/Al (100 nm). **Figure 4**a shows the spectra of the WOLEDs with a 2 nm thickness of $Ir(ppy)_3$:CDBP. Although three main peaks centered at 475, 512 and 616 nm could still be observed, the green and blue peaks were too close to each other with a wavelength separation of only 37 nm, while the green and red peaks were too far apart, with a separation of 104 nm, resulting in a deep valley between the green and red emissions. Thus, it is difficult to achieve a good color-rendering capability in such a three-emitter system due to the uneven separation of the emission peaks. To address this problem, at least one more yellow emitter has to be employed to compensate the spectra for the white-color deficiency,[13–15] which inevitably increases the complexity of the system. In addition, in contrast to the WOLEDs using **1** as the emitter, in which the spectra were less sensitive to the thickness of the green-emission layer, the spectra of the WOLEDs with $Ir(ppy)_3$ were found to be more sensitive. Due to the vicinity of the blue and green peaks, the green spectrum was actually the superimposition of both emission peaks of $Ir(ppy)_3$ and the tail emission of FIrPic. Thus, its intensity increased dramatically with an increase of the thickness of the green-emission layer, resulting in an unbalanced white emission, as shown in Figure 4b. For example, the CIE coordinates shifted from the white region of (0.32, 0.44) for the devices with the 2 nm thickness of $Ir(ppy)_3$:CDBP layer to the green region of (0.28, 0.53) for the devices with the 4 nm thickness of the $Ir(ppy)_3$:CDBP layer. Thus, to obtain a balanced white emission in such a three-emitter system, the thickness of the green emission layer has to be controlled carefully, which further increases the complexity of the fabrication process for practical use.

Figure 5a shows typical *J–V–L* characteristics of the devices. The current density decreased slightly with an increase of the thicknesses of the yellowish-green- or green-emission layers, which was expected due to the larger resistance induced by the thicker layer. All of the devices turned on at 4 V for 1 cd m^{-2}; however, at higher voltages, the devices with thicker yellowish-green layers exhibited a higher luminance. For example, at a driving voltage of 15 V, the luminance increased from 9829 cd m^{-2} for the devices without the **1**:CDBP layer to 20 024 cd m^{-2} and 24 090 cd m^{-2} for the devices with the 2 nm- and

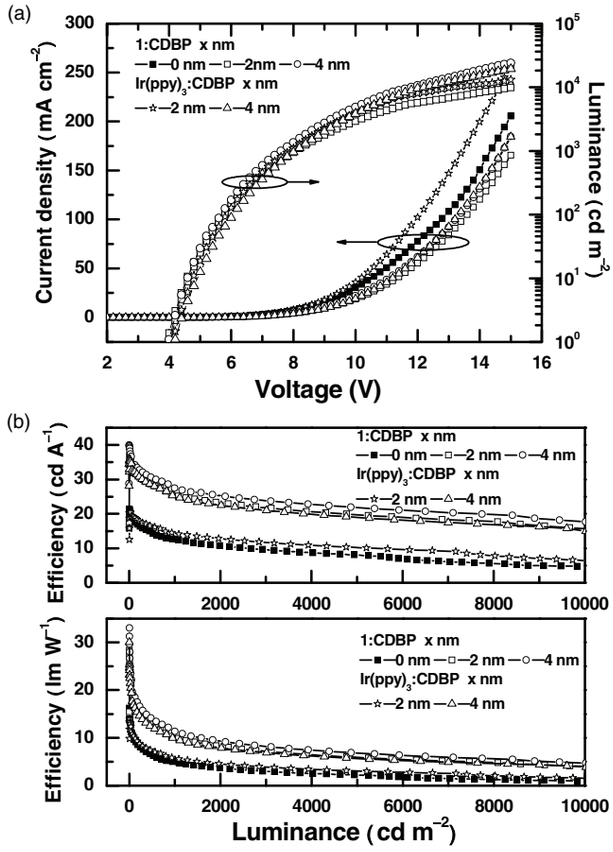

Figure 5. a) Current-density–luminance–voltage characteristics of the electrophosphorescent WOLEDs with different thickness of the yellowish green/green emission layer. b) Efficiency–luminance characteristics of the electrophosphorescent WOLEDs with different thickness of the yellowish green/green emission layer.

4 nm-thick **1**:CDBP layers, respectively, mainly owing to the high efficiency of the green emission. To verify this assertion, the efficiency–luminance characteristics are plotted in Figure 5b. Obviously, the devices with thicker yellowish-green-emission layers showed a higher EL efficiency. For example, at a luminance of 100 cd m^{-2}, the devices with the 4 nm-thick **1**:CDBP layer showed a high efficiency of 34.2 cd A^{-1} (13.2% and 18.5 lm W^{-1}), which is higher than the 31.8 cd A^{-1} (12.8% and 17.2 lm W^{-1}) and 17.9 cd A^{-1} (10.9% and 9.7 lm W^{-1}) for the devices with the 2 nm- and 0 nm-thick **1**:CDBP layers, respectively. In this case, the peak LE was 39.9 cd A^{-1}, corresponding to a peak PE of 33.0 lm W^{-1} and an EQE of 15.5%. The efficiency roll-off occurred quickly at high luminance; for example, at a high luminance of 1000 cd m^{-2}, the efficiency was 27.4 cd A^{-1} (10.7% and 11.3 lm W^{-1}), which is about 69% of its peak value, and is mainly due to the triplet-triplet annihilation and/or exciton leakage at high current density, a typical phenomenon in phosphorescent OLEDs. To address this issue, emitters with short exciton lifetimes may be adopted, device structures with a wide exciton recombination zone to reduce the exciton density can be designed,[27] and/or exciton-blocking layers with high triplet energy level can be employed to prevent exciton leakage at high current density.[28]

It should also be noted that the efficiencies of the devices doped with **1** were substantially higher than those with the $Ir(ppy)_3$ emitter; for example, at a luminance of 100 cd m^{-2}, the efficiency of the devices with the 2 nm-thick **1**:CDBP layer exhibited a high efficiency of 31.8 cd A^{-1} (12.8% and 17.2 lm W^{-1}), remarkably higher than the 19.1 cd A^{-1} (8.9% and 10.4 lm W^{-1}) for the devices with the 2 nm thickness of $Ir(ppy)_3$:CDBP, which was expected due to the higher efficiency of **1** than that of $Ir(ppy)_3$. The key characteristics of the devices are listed in **Table 3**. When these WOLEDs are used for solid-state lighting, all of the photons should be taken into account for illumination since the originally trapped photons can be redirected to the forward-viewing direction by applying light out-coupling techniques such as by engineering the lighting fixtures,[2d] roughing the substrate[29] or patterning a micro-lens array.[30] It has been experimentally shown that the efficiency can be improved by a factor of 1.2–2.3[31] if certain light out-coupling techniques are employed. Under these conditions, a maximal total LE of ≈71.8 cd A^{-1} and a maximal total PE of ≈59.4 lm W^{-1} can be obtained if a factor of 1.8 is adopted.

Table 3. Key performance characteristics of the electrophosphorescent WOLEDs with different yellowish-green/green-emission-layer thicknesses.

Structure	Thickness [nm]	V_{on} [V]	L_{max} @ 15 V [cd m^{-2}]	η_{ext} [%]	η_L [cd A^{-1}]	η_P [lm W^{-1}]	CIE co-ordinates [x, y]
With **1**	0	4	9829	10.9[a]	17.9	9.7	(0.35, 0.38)[c]
				7.7[b]	12.7	5.0	(0.33, 0.38)[d]
	2	4	20 024	12.8[a]	31.8	17.2	(0.35, 0.46)[c]
				10.2[b]	25.2	9.9	(0.34, 0.46)[d]
	4	4	24 090	13.2[a]	34.2	18.5	(0.34, 0.46)[c]
				10.7[b]	27.4	11.3	(0.33, 0.46)[d]
With $Ir(ppy)_3$	2	4.2	13 021	8.9[a]	19.1	10.4	(0.32, 0.44)[c]
				6.8[b]	14.5	5.8	(0.30, 0.43)[d]
	4	4.2	19 384	12.0[a]	32.2	16.3	(0.28, 0.53)[c]
				9.4[b]	25.3	9.9	(0.28, 0.51)[d]

[a]Values collected at 100 cd m^{-2}; [b]Values collected at 1000 cd m^{-2}; [c]Values collected at 6 V; [d]Values collected at 8 V.

Although high-efficiency WOLEDs with three evenly separated peaks have been demonstrated in the three-emitter system by employing **1** as a yellowish-green emitter, one may note that the CIE coordinates of (0.34, 0.46) of such WOLEDs are still far away from the equal-energy-white-point, which has to be improved for high-quality-illumination applications. In addition, the sky-blue emission stemming from FIrPic is far from saturation, which would significantly reduce the color gamut of a display. To alleviate these problems, a fluorescent emitter, BCzVBi, was adopted to replace the FIrPic as the deep-blue emitter. Hybrid WOLEDs were fabricated with a structure of ITO/NPB (40 nm)/10% $Ir(btp)_2(acac)$:CDBP (10 nm)/4% **1**:CDBP (4 nm)/CDBP (3 nm)/10% BCzVBi:CDBP (5 nm)/TAZ (40 nm)/LiF (1 nm)/Al (100 nm), where a 3 nm thickness of CDBP was inserted between the BCzVBi, the fluorescent emitter, and **1**, the phosphorescent emitter, to confine the singlet exciton recombining in the BCZVBi:CDBP region. With such an arrangement, both singlet and triplet excitons were expected to be harvested.[32,33] For comparison, WOLEDs were also fabricated with the commercial green emitter $Ir(ppy)_3$, with a structure of ITO/NPB (40 nm)/10% $Ir(btp)_2(acac)$:CDBP (10 nm)/7% $Ir(ppy)_3$:CDBP (4 nm)/CDBP (3 nm)/10% BCzVBi:CDBP (5 nm)/TAZ (40 nm)/LiF (1 nm)/Al (100 nm). **Figure 6** shows the EL spectra of these devices with **1** and $Ir(ppy)_3$. By adopting the deep-blue emitter, BCzVBi, both types of WOLED emitted a very-pure white color with CIE coordinates of (0.32, 0.34) and a color-correlated temperature (CCT) of 6042 K for the devices with **1** and (0.31, 0.32) and 6984 K, repectively, for the devices with $Ir(ppy)_3$. Although the CIE coordinates of both kinds of WOLED are close, the WOLEDs with **1** exhibited a significantly higher color-rendering capability as compared with those with $Ir(ppy)_3$. For example, the WOLEDs with **1** showed a respectably high CRI of 91.2, remarkably higher than the 63.6 for WOLEDs with $Ir(ppy)_3$. The high CRI was mainly caused by the three evenly separated emission peaks, which desirably covered the whole visible spectra. It is impressive that our best devices are superior to most currently known RGB-designed WOLEDs, showing a concomitant set of high-efficiency and CRI values (see Supporting Information). The poor CRI reported in the literature is attributable to the deep valley present between the green and red peaks: it is therefore important to select appropriate emitters with each emission peak separated evenly so that a high CRI can be attained, which is appropriate to indoor-lighting applications.

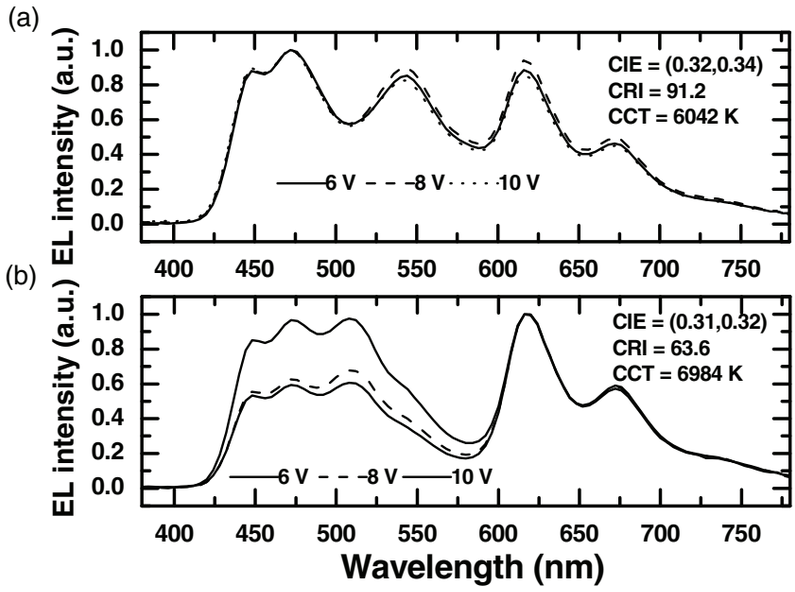

Figure 6. a,b) EL spectra of the hybrid WOLEDs with **1** (a) and $Ir(ppy)_3$ (b) as the emitters.

3. Conclusions

In conclusion, efficient WOLEDs with three evenly separated peaks have been demonstrated in a new three-emitter platform. In such a system, WOLEDs based on a tailor-made yellowish-green emitter, **1**, with a high synthetic accessibility demonstrated a remarkably higher efficiency together with an excellent color-rendering capability, as compared with the commercial benchmark green emitter $Ir(ppy)_3$. This is mainly attributable to the higher efficiency and red-shifted spectrum of **1** over that of $Ir(ppy)_3$. Our WOLEDs outperform most white-emitting RGB devices that have been reported in the literature, with a simultaneous enhancement of both WOLED efficiency and color rendition. The efficient WOLEDs, here with separated R, G and B peaks and a high color-rendering index of up to 91, would be ideal candidates to bring OLEDs into the next generation of full-color displays and the solid-state lighting market.

4. Experimental Section

General Information: All of the reactions were performed under nitrogen. The solvents were carefully dried and distilled from appropriate drying agents prior to use. Commercially available reagents were used without further purification unless otherwise stated. All of the reactions were monitored by TLC with Merck precoated glass plates. Flash column chromatography and preparative TLC were carried out on silica gel from Merck (0.063–0.200 mm). FAB-MS was carried out using a Finnigan MAT SSQ710 system. The NMR spectra were measured in $CDCl_3$ using a Bruker Ultrashield 400 MHz FT-NMR spectrometer; the ^1H and ^{13}C chemical shifts are quoted relative to the internal standard, tetramethylsilane.

Physical Measurements: UV–vis spectra were obtained using an HP-8453 spectrophotometer. The photoluminescent properties and lifetimes of the compounds were probed using a Photon Technology International (PTI) Fluorescence Master Series QM1 system. The phosphorescence quantum yields were determined in CH_2Cl_2 solution at 293 K against $Ir(ppy)_3$ as a reference ($\Phi_P = 0.40$).[34] Electrochemical measurements were made using a CHI model 600C electrochemistry station. A conventional three-electrode configuration, consisting of a platinum working electrode, a Pt-wire counter electrode and a Ag/AgCl reference electrode, was used. The supporting electrolyte was

0.1 M $[Bu_4N]PF_6$ in MeCN. All of the potentials reported are quoted with reference to the ferrocene-ferrocenium (Fc/Fc^+) couple at a scan rate of 100 mV s^{-1}. The oxidation potential (E_{ox}) was used to determine the HOMO energy level using the equation: HOMO $=-(E_{ox} + 4.8)$ eV, which was calculated using the reference standard ferrocene value of –4.8 eV with respect to vacuum.[24] Thermal analyses were performed using a Perkin–Elmer TGA6 thermal analyzer.

Preparation of Ligand ***HL1***: $Pd(PPh_3)_4$ (160 mg) was added to a mixture of 4-methylphenylboronic acid (1.07 g, 7.88 mmol), 2-chloro-5-(trifluoromethyl)pyridine (0.48 mg, 2.62 mmol) in toluene (50 mL) and a 2 M aqueous solution of Na_2CO_3 (8 mL) under an inert atmosphere of nitrogen. The reaction mixture was heated at 110 °C for 48 h. After cooling to room temperature, water was added and the solution mixture was extracted with ethyl acetate. The combined organic layer was dried over Na_2SO_4, filtered, and concentrated under reduced pressure. The residue was purified on a silica column by gradient elution with a mixture of hexane and CH_2Cl_2 (2:1, v/v) to afford a white solid (93%, 574 mg).

^{1}H NMR (400 MHz, $CDCl_3$, δ): 8.92 (s, 1H, Ar), 7.96–7.92 (m, 3H, Ar), 7.82–7.80 (d, J = 8.6 Hz, 1H, Ar), 7.32–7.30 (d, J = 8.1 Hz, 2H, Ar), 2.42 (s, 3H, CH_3); ^{13}C NMR (100 MHz, $CDCl_3$, δ): 160.65, 146.51, 140.31, 135.17, 133.80, 129.70, 127.14, 119.58 (Ar), 124.95, 124.62, 124.29, 123.96 (CF_3), 21.33 (CH_3); FAB-MS (m/z): 238.2 $[M]^+$.

Preparation of ***1***: $IrCl_3{\cdot}nH_2O$ (137 mg, 0.46 mmol) was allowed to react with the cyclometalating ligand **HL1** (275 mg, 1.16 mmol) in a mixture of 2-ethoxyethanol and water (3:1, v/v). The mixture was refluxed for 24 h and then cooled to room temperature. A precipitate gradually formed during the reaction, which was collected by filtration and washed with ethanol followed by hexane. The solid was then pumped dry completely to give the crude Ir(III) dimer for the subsequent reaction without further purification. This crude dimer was mixed with acetylacetone (0.05 mL) and Na_2CO_3 (173 mg, 1.63 mmol) in 2-ethoxyethanol (8 mL) and the reaction mixture was then refluxed for 16 h. After the mixture was cooled to room temperature, water was added and it was extracted with CH_2Cl_2. The organic layer was collected and the solvent was subsequently removed. The residue was then purified with preparative TLC plates using a mixture of hexane and CH_2Cl_2 (1:1, v/v) as eluent and product **1** was obtained as an orange powder in a 44% yield (156 mg).

^{1}H NMR (400 MHz, $CDCl_3$, δ): 8.71 (s, 2H, Ar), 7.91–7.90 (d, J = 1.4 Hz, 4H, Ar), 7.52–7.50 (d, J = 8.8 Hz, 2H, Ar), 6.70–6.68 (m, 2H, Ar), 6.04 (s, 2H, Ar), 5.25 (s, 1H, acac), 2.08 (s, 6H, CH_3), 1.80 (s, 6H, CH_3); ^{13}C NMR (100 MHz, $CDCl_3$, δ): 185.35 (CO), 172.08, 149.40, 145.22, 140.87, 140.33, 125.26, 125.02, 123.67, 122.73, 117.71 (Ar), 124.99, 124.28, 123.64, 123.30 (CF_3), 100.85 (CH), 28.61 (CH_3), 21.83 (CH_3); FAB-MS (m/z): 764.2 $[M]^+$; Anal. calcd (%) for $C_{31}H_{25}N_2F_6O_2Ir$: C 48.75, H 3.30, N 3.67; found: C 48.96, H 3.58, N 3.85.

Device Fabrication and Testing: The devices were fabricated on 80 nm-ITO-coated glass with a sheet resistance of 25 Ω per square. Prior to loading into the pretreatment chamber, the ITO-coated glass was soaked in an ultrasonic detergent for 30 min, followed by spraying with deionized water for 10 min, soaking in ultrasonic deionized water for 30 min and oven-baking for 1 h. The cleaned samples were treated with CF_4 plasma at a power of 100 W, a gas flow of 50 sccm and a pressure of 0.2 Torr for 10 s in the pretreatment chamber. Then, the samples were transferred to the organic chamber with a base pressure of 5×10^{-7} Torr without breaking the vacuum for depositing the organic layer. The samples were then transferred to a metal chamber for cathode deposition, which was composed of 1 nm LiF capped with 100 nm Al. The light-emitting area was 4 mm^2 as defined by the overlap of the cathode and anode. The current-density–voltage characteristics of the devices were measured using an HP4145B semiconductor parameter analyzer. The forward-direction photons emitted from the devices were detected using a calibrated UDT PIN-25D silicon photodiode. The luminance and external quantum efficiency of the devices were inferred from the photocurrent of the photodiode. The electroluminescent (EL) spectra were obtained using a PR650 spectrophotometer. All of the measurements were carried out under air at room temperature without device encapsulation.

Supporting Information

Supporting Information is available from the Wiley Online Library or from the author.

Acknowledgements

S.C. and G.T. contributed equally to this work. The work was supported by the Hong Kong Research Grants Council (HKBU202709 and HKUST2/CRF/10), the University Grants Committee of HKSAR, China (AoE/P-03/08) and Hong Kong Baptist University (FRG2/10-11/101). We thank Prof. W.-H. Leung and Mr. V. H.-Y. Ng at the Hong Kong University of Science & Technology for assistance in the electrochemical studies of **1**.

Received: April 21, 2011
Published online: August 3, 2011

[1] a) S. Chen, Z. Zhao, B.-Z. Tang, H.-S. Kwok, *J. Phys. D: Appl. Phys.* **2010**, *43*, 095101; b) S. Chen, Z. Zhao, Z. Wang, P. Lu, Z. Gao, Y. Ma, B.-Z. Tang, H.-S. Kwok, *J. Phys. D: Appl. Phys.* **2011**, *44*, 145101.

[2] a) H. B. Wu, L. Ying, W. Yang, Y. Cao, *Chem. Soc. Rev.* **2009**, *38*, 3391; b) Q. Wang, D. Ma, *Chem. Soc. Rev.* **2010**, *39*, 2387; c) M. C. Gather, A. Köhnen, K. Meerholz, *Adv. Mater.* **2011**, *23*, 233; d) B. W. D'Andrade, S. R. Forrest, *Adv. Mater.* **2004**, *16*, 1585; e) G. Zhou, W.-Y. Wong, S. Suo, *J. Photochem. Photobiol. C: Photochem. Rev.* **2010**, *11*, 133; f) G. M. Farinola, R. Ragni, *Chem. Soc. Rev.* **2011**, *40*, 3467; g) W.-Y. Wong, C.-L. Ho, *J. Mater. Chem.* **2009**, *19*, 4457; h) W.-Y. Wong, C.-L. Ho, *Coord. Chem. Rev.* **2009**, *253*, 1709; i) J. Zou, H. Wu, C.-S. Lam, C. Wang, J. Zhu, C. Zhong, S. Hu, C.-L. Ho, G.-J. Zhou, H. Wu, W. C. H. Choy, J. Peng, Y. Cao, W.-Y. Wong, *Adv. Mater.* **2011**, *23*, 2976.

[3] Q. Wang, J. Ding, D. Ma, Y. Cheng, L. Wang, X. Jing, F. Wang, *Adv. Funct. Mater.* **2009**, *19*, 84.

[4] S. Chen, H.-S. Kwok, *Org. Electron.* **2011**, *12*, 677.

[5] S. Reineke, F. Lindner, G. Schwartz, N. Seidler, K. Walzer, B. Lüssem, K. Leo, *Nature* **2009**, *459*, 234.

[6] B. W. D'Andrade, R. J. Holmes, S. R. Forrest, *Adv. Mater.* **2004**, *16*, 624.

[7] Y. Sun, S. R. Forrest, *Appl. Phys. Lett.* **2007**, *91*, 263503.

[8] G. Cheng, Y. Zhang, Y. Zhao, Y. Lin, C. Ruan, S. Liu, T. Fei, Y. Ma, Y. Cheng, *Appl. Phys. Lett.* **2006**, *89*, 043504.

[9] S.-H. Eom, Y. Zheng, E. Wrzesniewski, J. Lee, N. Chopra, F. So, J. Xue, *Appl. Phys. Lett.* **2009**, *94*, 153303.

[10] a) X. Zhu, J. Sun, X. Yu, M. Wong, H.-S. Kwok, *J. Appl. Phys.* **2007**, *46*, 4054; b) G. Zhou, Q. Wang, C.-L. Ho, W.-Y. Wong, D. Ma, L. Wang, *Chem. Commun.* **2009**, 3576.

[11] C.-H. Chang, H.-C. Cheng, Y.-J. Lu, K.-C. Tien, H.-W. Lin, C.-L. Lin, C.-J. Yang, C.-C. Wu, *Org. Electron.* **2010**, *11*, 247.

[12] M. Kashiwabara, K. Hanawa, R. Asaki, I. Kobori, R. Matsuura, H. Yamada, T. Yamamoto, A. Ozawa, Y. Sato, S. Terada, J. Yamada, T. Sasaoka, S. Tamura, T. Urabe, *Dig. Tech. Pap - Soc. Inf. Disp. Int. Symp.* **2004**, *35*, 1017.

[13] a) X. M. Yu, G. J. Zhou, C.-S. Lam, W.-Y. Wong, X. L. Zhu, J. X. Sun, M. Wong, H.-S. Kwok, *J. Organomet. Chem.* **2008**, *693*, 1518; b) S. Murano, E. Kucur, G. He, J. Blochwitz-Nimoth, T. K. Hatwar, J. Spindler, S. Van Slyke*Dig. Tech. Pap - Soc. Inf. Disp. Int. Symp.* **2009**, *40*, 417.

[14] J.-H. Jou, Y.-C. Chou, *Dig. Tech. Pap - Soc. Inf. Disp. Int. Symp.* **2010**, *41*, 1902.

[15] Y.-S. Park, J.-W. Kang, D.-M. Kang, J.-W. Park, Y.-H. Kim, S.-K. Kwon, J.-J. Kim, *Adv. Mater.* **2008**, *20*, 1957.

[16] a) S. Aoki, Y. Matsuo, S. Ogura, H. Ohwada, Y. Hisamatsu, S. Moromizato, M. Shiro, M. Kitamura, *Inorg. Chem.* **2011**, *50*, 806; b) J. Li, P. I. Djurovich, B. D. Alleyne, M. Yousufuddin, N. N. Ho, J. Christopher Thomas, J. C. Peters, R. Bau, M. E. Thompson, *Inorg. Chem.* **2005**, *44*, 1713; c) V. V. Grushin, N. Herron, D. D. LeCloux, W. J. Marshall, V. A. Petrov, Y. Wang, *Chem. Commun.* **2001**, 1494.

[17] N. Miyaura, A. Suzuki, *Chem. Rev.* **1995**, *95*, 2457.

[18] S. Lamansky, P. Djurovich, D. Murphy, F. Abdel-Razzaq, R. Kwong, I. Tsyba, M. Bortz, B. Mui, R. Bau, M. E. Thompson, *Inorg. Chem.* **2001**, *40*, 1704.

[19] a) W.-Y. Wong, G.-J. Zhou, X.-M. Yu, H.-S. Kwok, Z.-Y. Lin, *Adv. Funct. Mater.* **2007**, *17*, 315; b) C.-L. Ho, W.-Y. Wong, Z.-Q. Gao, C.-H. Chen, K.-W. Cheah, B. Yao, Z.-Y. Xie, Q. Wang, D.-G. Ma, L.-X. Wang, X.-M. Yu, H.-S. Kwok, Z.-Y. Lin, *Adv. Funct. Mater.* **2008**, *18*, 319; c) F. O. Garces, K. A. King, R. J. Watt, *Inorg. Chem.* **1998**, *27*, 3464. d) Y. Wang, N. Herron, V. V. Grushin, D. LeCloux, V. Petrov, *Appl. Phys. Lett.* **2001**, *79*, 449.

[20] A. B. Tamayo, S. Garon, T. Sajoto, P. I. Djurovich, I. M. Tsyba, R. Bau, M. E. Thompson, *Inorg. Chem.* **2005**, *44*, 8723.

[21] L. L. Han, D. F. Yang, W. L. Li, B. Chu, Y. R. Chen, Z. S. Su, D. Y. Zhang, F. Yan, S. H. Wu, J. B. Wang, Z. Z. Hu, Z. Q. Zhang, *Appl. Phys. Lett.* **2009**, *94*, 163303.

[22] a) M. A. Baldo, C. Adachi, S. R. Forrest, *Phys. Rev. B: Condens. Matter* **2000**, *62*, 10967; b) E. B. Namdas, A. Ruseckas, D. W. Samuel, S. C. Lo, P. L. Burn, *Appl. Phys. Lett.* **2005**, *86*, 091104; c) G.-J. Zhou, W.-Y. Wong, B. Yao, Z. Xie, L. Wang, *J. Mater. Chem.* **2008**, *18*, 1799.

[23] C.-L. Ho, W.-Y. Wong, G.-J. Zhou, B. Yao, Z.-Y. Xie, L.-X. Wang, *Adv. Funct. Mater.* **2007**, *17*, 2925.

[24] a) M. Thelakkat, H.-W. Schmidt, *Adv. Mater.* **1998**, *10*, 219; b) R. S. Ashraf, M. Shahid, E. Klemm, M. Al-Ibrahim, S. Sensfuss, *Macromol. Rapid Commun.* **2006**, *27*, 1454; c) C.-L. Ho, Q. Wang, C.-S. Lam, W.-Y. Wong, D. G. Ma, L. X. Wang, Z.-Q. Gao, C.-H. Chen, K.-W. Cheah, Z. Lin, *Chem. Asian J.* **2009**, *4*, 89.

[25] a) S. Tokito, T. Iijima, Y. Suzuri, H. Kita, T. Tsuzuki, F. Sato, *Appl. Phys. Lett.* **2003**, *83*, 569; b) S. Takizawa, V. A. Montes, P. Anzenbacher Jr., *Chem. Mater.* **2009**, *21*, 2452.

[26] a) S. M. King, H. A. Al-Attar, R. J. Evans, A. Congreve, A. Beeby, A. P. Monkman, *Adv. Funct. Mater.* **2006**, *16*, 1043; b) Y.-C. Chiu, J.-Y. Hung, Y. Chi, C.-C. Chen, C.-H. Chang, C.-C. Wu, Y.-M. Cheng, Y.-C. Yu, G.-H. Lee, P.-T. Chou, *Adv. Mater.* **2009**, *21*, 2221; c) P.-T. Chou, Y. Chi, *Chem. Eur. J.* **2007**, *13*, 380; d) Y. Chi, P.-T. Chou, *Chem. Soc. Rev.* **2010**, *39*, 638.

[27] S. H. Kim, J. Jang, K. S. Yook, J. Y. Lee, *Appl. Phys. Lett.* **2008**, *92*, 023513.

[28] S.-J. Su, E. Gonmori, H. Sasabe, J. Kido, *Adv. Mater.* **2008**, *20*, 4189.

[29] a) S. Chen, H. -S. Kwok, *Opt. Express* **2010**, *18*, 37; b) J Zhou, N. Ai, L. Wang, H. Zheng, C. Luo, Z. Jiang, S. Yu, Y. Cao, J. Wang, *Org. Electron.* **2011**, *12*, 648.

[30] S. Möller, S. R. Forrest, *J. Appl. Phys.* **2002**, *91*, 3324.

[31] K. Saxena, V. K. Jain, D. S. Mehta, *Opt. Mater.* **2009**, *32*, 221.

[32] Y. Sun, N. C. Giebink, H. Kanno, B. Ma, M. E. Thompson, S. R. Forrest, *Nature* **2006**, *440*, 908.

[33] G. Schwartz, S. Reineke, T. C. Rosenow, K. Walzer, K. Leo, *Adv. Funct. Mater.* **2009**, *19*, 1319.

[34] a) K. A. King, P. J. Spellane, R. J. Watts, *J. Am. Chem. Soc.* **1985**, *107*, 1431; b) H. Wu, G. Zhou, J. Zou, C.-L. Ho, W.-Y. Wong, W. Yang, J. Peng, Y. Cao, *Adv. Mater.* **2009**, *21*, 4181.